Superlattices and Microstructures 162 (2022) 107132

Contents lists available at ScienceDirect

Superlattices and Microstructures

journal homepage: www.elsevier.com/locate/superlattices

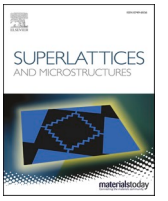

First-principles calculations to investigate electronic structure and optical properties of 2D $MgCl_2$ monolayer

H.R. Mahida [a], Abhishek Patel [a], Deobrat Singh [b,*], Yogesh Sonvane [c], P. B. Thakor [a,**], Rajeev Ahuja [b,d]

[a] Department of Physics, Veer Narmad South Gujarat University, Surat, 35007, India
[b] Condensed Matter Theory Group, Materials Theory Division, Department of Physics and Astronomy, Uppsala University, Box 516, 75120, Uppsala, Sweden
[c] Advanced Material Lab, Department of Physics, Sardar Vallabhbhai National Institute of Technology, Surat, 395007, India
[d] Department of Physics, Indian Institute of Technology Ropar, Rupnagar, 140001, Punjab, India

ARTICLE INFO

Keywords:
2D monolayer $MgCl_2$ material
Structural stability
Phonon dispersion
Electronic properties
Optical properties
First-principles calculations

ABSTRACT

In the present work, we have concentrated on the structural, electronic, and optical properties of single-layer phase $MgCl_2$. When bulk $MgCl_2$ reduces to monolayer form, then it exhibited indirect to direct bandgap transformation. The result indicates that the monolayer $MgCl_2$ exhibits insulating characteristics with a direct bandgap of 7.377 eV whereas its bulk form has an indirect bandgap of 7.02 eV. It means that when reducing the dimensionally of the $MgCl_2$ materials than its bandgap significantly increased. The optical properties of the monolayer $MgCl_2$ have been investigated using DFT within the random phase approximation. The calculated refractive index values are very near to water, which means that monolayer $MgCl_2$ material will be a transparent material. Also, the optical absorption coefficient is found to be very high in the ultraviolet (UV) region. From optical properties, the out-of-plane ($E\perp Z$) direction of polarizations is shifted towards the higher photon energy as compared to the in-plane ($E||X$) direction. From the optical properties profile, the polarizations along in-plane and out-of-plane are different therefore it shows anisotropic behavior. These investigated results show the monolayer $MgCl_2$ could be a promising material for optoelectronic nanodevices such as deep UV emitters and detectors, electrical insulators, atomically thin coating materials.

1. Introduction

In the fields of nanoscience and nano-technology, the various family of two-dimensional (2D) materials have been hopeful candidates with innovative and novel properties for new devices with high performance [1–3]. Specifically, the isolated graphene monolayer sheets with unique and novel properties have provided an excellent platform at nano-scale with potential applications [4–6]. The other 2D such as important monolayer, the MoS_2, transition-metal dichalcogenides (TMDs), and many others like boron nitride, silicone, and phosphorene were successfully experimentally realized through various exfoliation methods [7–12]. Due to the innovative and novel properties, the transition metal dichalcogenides (TMD) monolayer such as MoX_2 and WX_2 (where X = S, Se, and

* Corresponding author.
** Corresponding author.
E-mail addresses: deobrat.singh@physics.uu.se (D. Singh), pbthakor@rediffmail.com (P.B. Thakor).

https://doi.org/10.1016/j.spmi.2021.107132
Received 3 August 2021; Received in revised form 11 December 2021; Accepted 26 December 2021
Available online 4 January 2022

Te) have been studied with special attention in the past decade [2,9,13–16]. Therefore, these materials have been enabled the platform for various applications such as nano-electronics, thermoelectric, optoelectronics, nano-science, bio-sensor, gas-sensor, transistors, valleytronics, and other applications [17–27]. In the present day, the many monolayers TMDs and transition metal halides (TMHs) with unique and novel properties can be utilized for specific applications [28–34]. Thus, the exploring and controlling of the electronic and optical properties of such materials play a crucial role in the various potential applications [35–40].

Furthermore, the halide group-based material has received considerable attention as the third generation of the semi-conductor and insulating materials [9,41–44]. The MgF_2 material has unique optical properties with high transparency over a wide range of photon energies. Magnesium fluoride (MgF_2) has increased in popularity to become the ideal anti-reflection coating for laser devices and is also an important material for optical fiber communication technology due to its wide bandgap, low refractive index, excellent mechanical properties, and high laser damage resistance [45,46]. The solution of magnesium fluoride (MgF_2) has been utilized as anti-reflective coatings material on the glass substrates with tunable properties by changing the particle size distribution, viscosity, and other structural parameters [47–49]. The 2D monolayer $MgCl_2$ is not a naturally available material and is an example of a transition metal halide (TMH) crystal. Due to the abundance of the bulk form in nature and smaller cleavage energy, the TMH with 2D layered has currently attracted research attention. These materials have been being ideal for exfoliation extraction similar to the TMDs.

Motivated by these interesting consequences, the structural, electronic, and optical properties of the monolayer $MgCl_2$ have been thoroughly investigated through first-principles calculations to explore it. The structural stability of the single-layer of $MgCl_2$ has been also examined via phonon band structure. In the electronic properties, the electronic band structure and projected density of states (PDOS) of $MgCl_2$ have been computed for single-layer and bulk phases. The optical properties of the 2D monolayer $MgCl_2$ such as frequency dependent real and imaginary part of the complex dielectric function, optical absorption coefficient, electron energy loss spectrum, refractivity, extinction coefficient, reflectivity, and transmittance have been also determined and studied.

1.1. Computational methods

The Density Functional Theory(DFT) computations have been executed utilizing the Vienna Ab initio Simulation Package (VASP) software [50,51]. The projector-augmented wave (PAW) method has been utilized with exchange-correlation (XC) function generalized gradient approach (GGA) of Perdew-Burke-Ernzerhof (PBE) within the plane wave cutoff having 500 eV [52,53]. The Monkhorst-Pack (MP) k-point grid of the size ($11 \times 11 \times 1$) has been employed for sampling the first Brillouin zone of monolayer $MgCl_2$ in the reciprocal space [54]. To prevent the interaction between the adjacent periodic layers, the vacuum of 20 Å has been used in the z-direction of the monolayer $MgCl_2$. The conjugate gradient (CG) technique has been utilized to optimize the structure with energy convergence criteria for total energy of 10^{-8} eV for self-consistent field (SCF) calculations and the Hellmann-Feynman(HF) forces converge criteria of 10^{-3} eV/Å . The electronic properties of the material are computed through the hybrid functional HSE06 with a mixing parameter (α) of 25% and a screening parameter of 0.2 $Å^{-1}$ [55–57]. The density functional perturbation theory (DFPT) computation was executed for $3 \times 3 \times 1$ sized supercell of the monolayer using the k-point mesh of ($2 \times 2 \times 1$) [58]. By utilizing these DFPT results, the Phonopy code has been utilized to determine the phonon dispersion for monolayer $MgCl_2$ [58,59]. And the ab-initio molecular dynamics (AIMD) calculations have been performed in the canonical (NVT) ensemble for $3 \times 3 \times 1$ supercell of this material at T = 300 K for 10 ps time period with an interval step of 2 fs to check the thermal stability. The frequency-dependent complex dielectric constant has been computed using the first principles computations based on DFT within the random phase approximation (RPA) and is used to evaluate and describe the optical properties of materials, where ε_1 and ε_2 are the real and imaginary parts of complex dielectric functions [49,60,61], respectively.

$$\varepsilon_1(\omega) = 1 + \frac{2}{\pi} p \int_0^{\infty} \frac{\omega' \varepsilon_2(\omega') d\omega'}{(\omega'^2 - \omega^2)}, \tag{1}$$

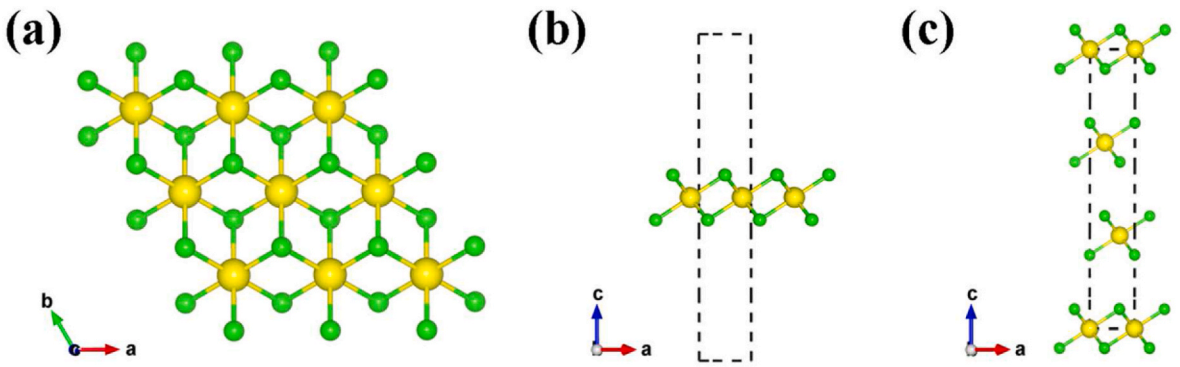

Fig. 1. (a) Top view of monolayer $MgCl_2$, (b) side view of 2D monolayer $MgCl_2$ and (c) bulk phase of $MgCl_2$. (Here, the yellow spheres for Mg atoms and green spheres for Cl atoms). (For interpretation of the references to colour in this figure legend, the reader is referred to the Web version of this article.)

$$\varepsilon_2(\omega) = \left(\frac{4\pi^2 e^2}{m^2\omega^2}\right)\sum_{i,j}\int_k \langle i|Mj\rangle^2 f_i(1-f_i) \times \delta\left(E_{j,k} - E_{i,k} - \omega\right)d^3k, \quad (2)$$

2. Results and discussion

2.1. Structural properties

Fig. 1 illustrates the optimized structures of the monolayer and bulk of the $MgCl_2$. In the structure of the bulk $MgCl_2$, the stacking of layer (Cl–Mg–Cl) have been bound by weak van der Waals interactions. The Mg and Cl atoms in the layer (Cl–Mg–Cl) has been strongly bounded by covalent bonds. The monolayer $MgCl_2$ can be prepared by isolation of single layer from a multi-layer form of bulk phase After optimizing the structure of monolayer $MgCl_2$, the lattice constants are to be $a = b = 3.670$ Å. While for the bulk phase of $MgCl_2$, the lattice constants are to be and $c = 19.72$ Å which has been good agreed with experimentally measured values lattice constant of bulk $MgCl_2$, 3.641 Å and 5.928 Å in a and c directions The bond angles $\alpha = \beta = 90^\circ$ and $\gamma = 120.0^\circ$, which validated its graphene-like structure (2D hexagonal). The bond length of the bond Mg–Cl is to be 2.793 Å.

The dynamic stability of the 2D monolayer-sheet $MgCl_2$ has been confirmed by the positive phonon dispersion. Here, the phonon dispersion of this monolayer is free from imaginary frequencies in the first Brillouin zone. Furthermore, we have examined the thermal stability of the monolayer $MgCl_2$ at 300 K by the AIMD calculations as shown in Fig. 2(b). The fluctuations in the total energy have been negligible small concerning time. The structural distortions as well as no breaking of bonds between the Mg–Cl atoms are not observed. Thus, the 2D monolayer $MgCl_2$ has a thermally stable material at room temperature. The dynamically and thermally of 2D $MgCl_2$ confirms the structural stability for the single-layer phase.

2.2. Electronic properties

Furthermore, the electronic band structures of the 2D $MgCl_2$ for bulk and monolayer phase have been determined as illustrated in Fig. 3(a, c). The bulk $MgCl_2$ shows the indirect bandgap of 7.07 eV between Γ and M in the valence band maximum (VBM) to Γ point in the conduction band minimum (CBM) (see Fig. 3(a)). While the monolayer $MgCl_2$ shows a direct bandgap of 7.38 eV (using HSE06 functional) and 5.959 eV (using PBE functional) Γ point. The calculated electronic bandgap has good consistent with previously reported investigations. Here, the $MgCl_2$ reduces its dimension from bulk form to monolayer, it has exhibited bandgap transition from indirect to direct (see Table 1).

To examine the orbital nature and electronic properties more thoroughly, the projected density of states (PDOS) of the 2D $MgCl_2$ has been determined for the monolayer form and bulk phase as shown in Fig. 3 (b,d). For the $MgCl_2$, the s orbital of the Mg atom and the p orbital of the Cl atom plays a crucial role in the formation of the total density of states. In the formation total density of states (TDOS) of the conduction band, the s orbital of the Mg atom has a major contribution while the p orbital of the Cl atom has a negligible contribution. But in the composition of the total density of states (TDOS) of the valence band, the p orbital of the Cl atom has a predominant contribution whereas the s orbital of the Mg atom has a negligible small contribution. The orbitals Mg(s) and Cl(p) plays a significant role in the formation of Mg–Cl covalent bonding.

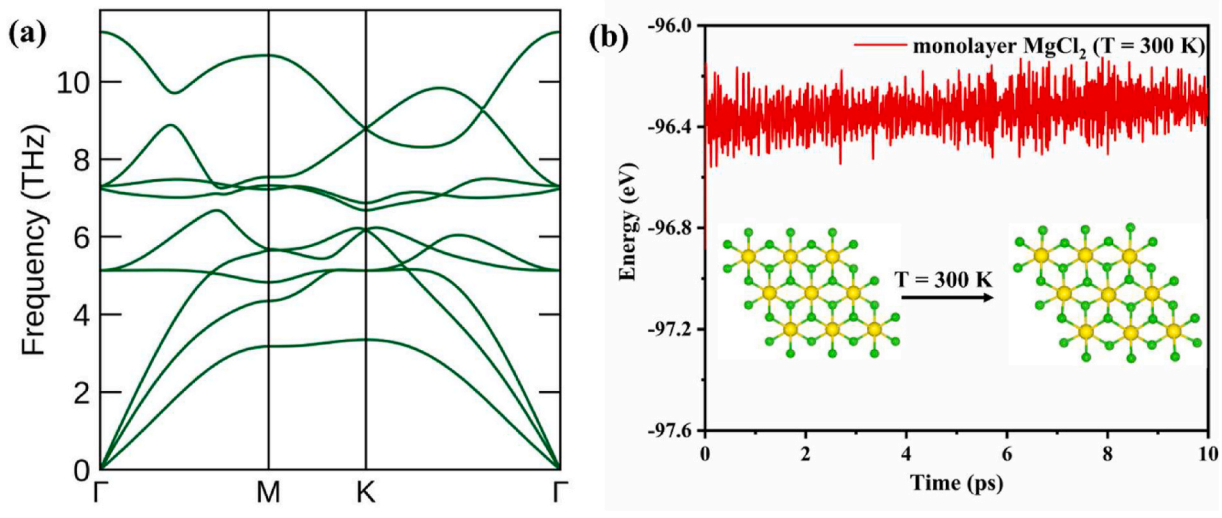

Fig. 2. (a) Phonon dispersion band-structure and (b) ab-initio molecular dynamics (AIMD) at T = 300 K for the single layer $MgCl_2$.

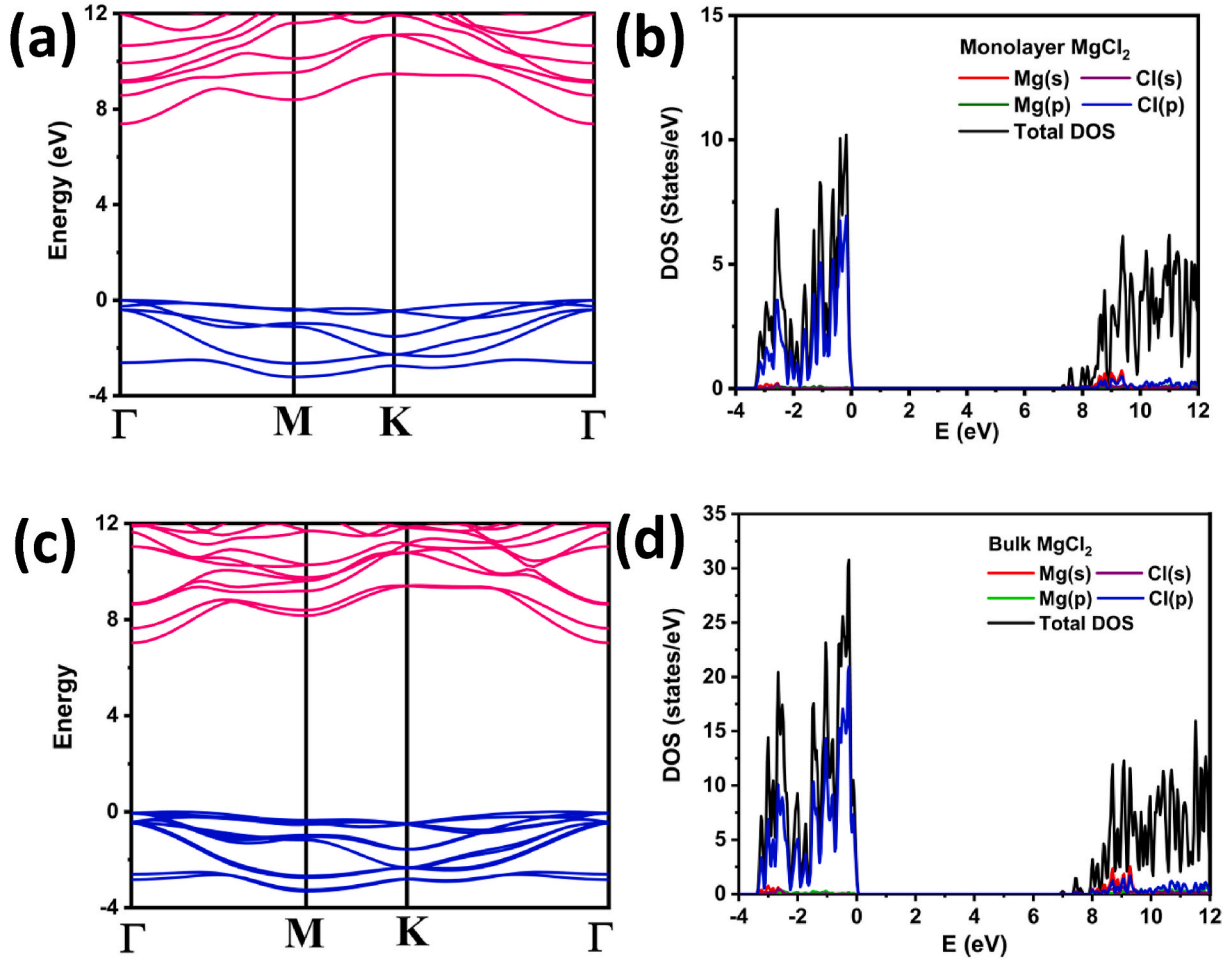

Fig. 3. (a) Electronic band-structure of monolayer $MgCl_2$ and (b) projected density of states of monolayer $MgCl_2$ (c) electronic band structure of bulk-$MgCl_2$ and (d) projected density of state of bulk-$MgCl_2$.

Table 1
Electronic bandgap in eV of $MgCl_2$ using HSE06 and PBE functionals.

Material	HSE		PBE	
	Direct bandgap	Indirect bandgap	Direct bandgap	Indirect Bandgap
$MgCl_2$ (monolayer)	7.38	_	5.96	_
$MgCl_2$ (bulk)	7.02	7.07	5.60	5.65

2.3. Optical properties

The complex frequency-dependent dielectric constant is also useful in determining the other optical characteristics of the materials such as optical absorption, electron energy loss spectra, refractivity, extinction coefficient, reflectivity, and transmittance [17,35]. Fig. 4 illustrates the real and imaginary parts of the dielectric constant for the monolayer $MgCl_2$. The electronic polarizability of the substance can be determined from the real part of the dielectric function by using the Clausius-Mossoti relation [62]. It means that the real part of the complex dielectric function tells us about the electronic polarizability of the materials. The real part of the complex dielectric function at zero photon energy is known as the static dielectric function (optical dielectric constant). Whereas the imaginary part of the complex dielectric function is concerned with the inter-band transition of electrons from the valence band to the conduction band. Fig. 4(a) shows that the static dielectric constant value is almost 1.54 for in-plane (E||X) and this value for out-of-plane (E⊥Z) is just about 1.50 eV. Also, it is clearly seen that the anisotropic behavior of optical properties because the real part of the dielectric function shows relatively larger electronic polarization along the in-plane direction as compared to the out-of-plane direction at lower photon energy up to 10 eV. There is one negative value in the range of 13.69 eV in the E⊥Z case for the single-layer sheet of $MgCl_2$. This denotes that the $MgCl_2$ monolayer reveals a metallic character for that photon energy. The mainly three peaks have been located at the

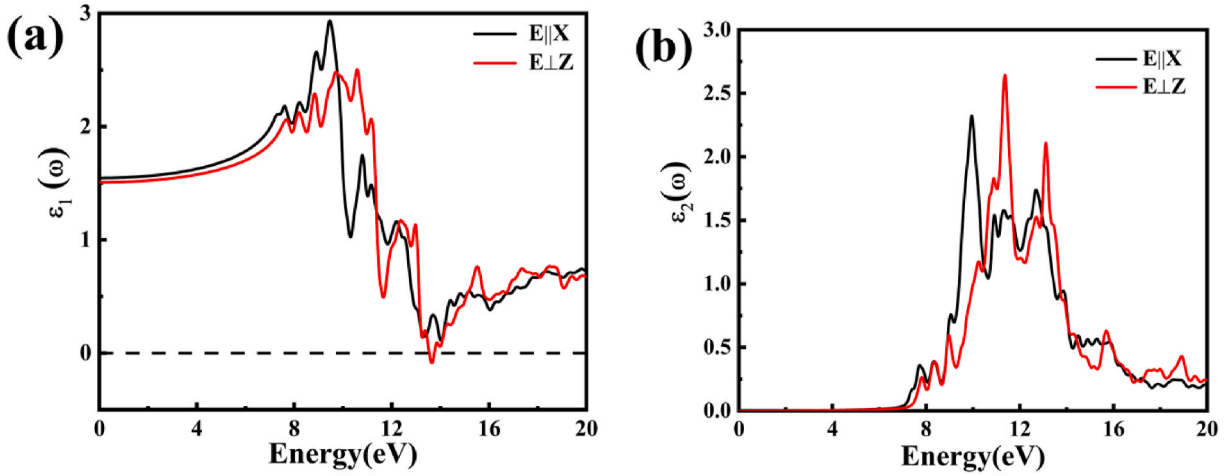

Fig. 4. (a) Real diectric function and (b) imaginary diectric function of the single layer $MgCl_2$.

energy's values in the polarization direction E||X is 9.48 eV, 10.82 eV, and 12.21 eV in the polarization, the direction is 10.62 eV, 12.36 eV, and 15.54 eV. The real part of the dielectric function's minimum value is around 14.00 eV for the parallel component and 13.65 eV for the perpendicular component of the $MgCl_2$ monolayer. The maximum electronic polarizability is found to be in the energy range of 9.48 eV (E||X) and 10.57 eV (E⊥Z) for the $MgCl_2$ single layer sheet.

The imaginary part of the complex dielectric function, which is directly related to interband transition is illustrated in Fig. 4(b). At low frequencies range of the imaginary portion of the dielectric function has no reaction to the electromagnetic radiation up to about 7.37 eV for parallel direction, and this value for perpendicular direction is almost 7.61 eV, so that, alongside with the outcome of DOS (Fig. 3(d)). It means that there is no inter-band transition that occurs from VBM to CBM up to the electronic bandgap. When the photon energy range increased beyond the electronic bandgap then an absorption peak appears (see Fig. 4(b)). The main peaks of the imaginary portion spread out over a broad scale of energy from 7.5 eV to 17.5 eV for both parallel and perpendicular polarization directions. From the imaginary part, we observe that threshold energy befell at 7.37 eV for the E||X case and 7.61 eV for (E⊥Z), which corresponds to the bandgap of the $MgCl_2$ monolayer. There is a prominent absorption peak at 9.93 eV for the parallel component and 11.36 eV for the perpendicular component; this peak is linked with the inter-band contributions. On the other hand, the primary and another exciton peak is present in the ultraviolet (UV) region. Agreeing to this, the monolayer system mainly absorbs the UV light, which signifies the $MgCl_2$ monolayer system is a potential applicant for UV absorption. Additionally, the noticeable absorption tips of the imaginary part of the dielectric constant shift to the lesser energies in the UV region and show high intensity with the blue shift.

Fig. 5 shows the computed frequency-dependent absorption coefficient with two different electric field orientations, which is also an essential parameter to estimate optical properties for optoelectronic applications. When an electromagnetic wave propagates per unit distance propagating in the medium, the percentage of light intensity attenuation during the wave's propagation is said to be the light absorption coefficient. The absorption coefficient is directly connected to both the imaginary fraction of the dielectric function and the extinction coefficient as shown in Figs. 4(b) and Fig. 6(b). The penetration depth of light in a given material is described as the

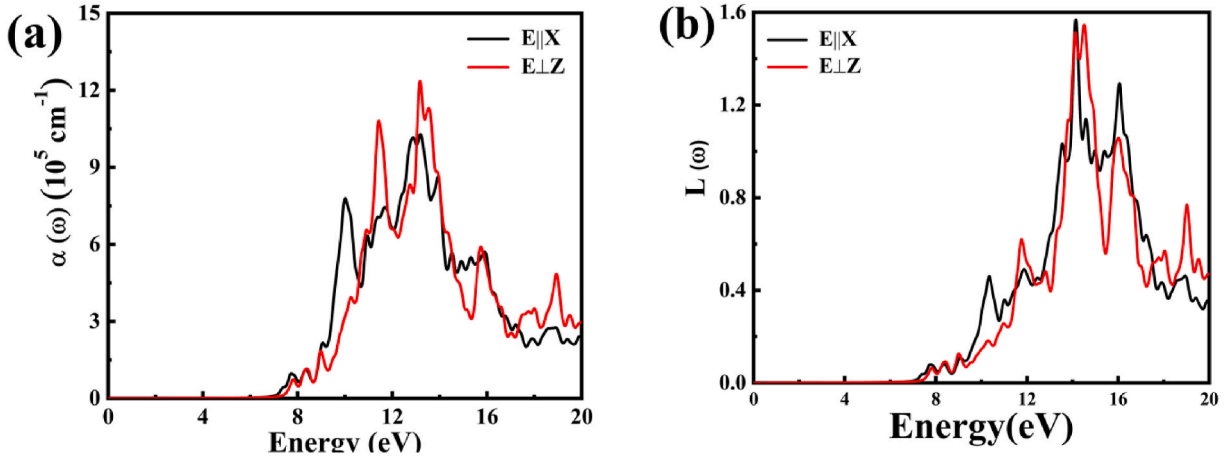

Fig. 5. (a) Absorption coefficient and (b) electron energy loss spectrum of monolayer $MgCl_2$.

absorption coefficient α(ω). Less light absorption leads to a lower absorption coefficient of the material. The first absorption peak appears at the energy of 7.74 eV and 7.84 eV relating to E||X and E⊥Z, respectively, and the uppermost absorption peak relates to the energy of 13.20 eV, which lies in the UV region. The absorption coefficient is inconsiderable at a low energy range of 7 eV. There are four fundamental peaks in E||X located at 10.03 eV, 11.76 eV 13.10 eV and 15.94 eV. In E⊥Z, we attained three tips; the first tip is at 7.84 eV; furthermore, at 11.46 eV and 13.20 eV, there are two tips with high α(ω). The high value of α (ω) of 1.27×10^6 cm^{-1} indicates that monolayer $MgCl_2$ has potential applications as a UV absorber.

The energy loss function L(ω) has been illustrated in Fig. 5(b). There are many sharp peaks located at about 10.33 eV, 13.50 eV, and 16.09 eV in the electric field parallel to single layer $MgCl_2$ sheet, and for E⊥Z polarization, sharp peaks occur around 11.76 eV, 16.04 eV, and 19.02 eV, which explained (π+σ) plasmon. There is no noticeable peak at energies below 7 eV under parallel and perpendicular polarizations. Some weak peak is observed between the energy ranges 7.00 eV–12 eV that are related to faint resonances of incidence light. For the $MgCl_2$ monolayer, in both E||X and E||Z polarization directions, all plasmonic peaks are swung toward greater energies and get sharper (blueshift) if the material reflects the frequency of electromagnetic radiation lower than plasma frequency because the electrons in substance effectively screen the electric field of radiation. It assumes that electromagnetic radiation's frequency exceeds that of plasma; it is transferred by the material when electrons in the material cannot screen it.

The refraction index and extinction coefficient of the $MgCl_2$ monolayer sheet have been illustrated in Fig. 6. Refractive index n(ω) denotes bending or refraction of light on interacting with the substance. Static refractive index values (the value of the refractive index at zero photon energy) of $MgCl_2$ monolayer for parallel and perpendicular components are 1.24 and 1.22, respectively. As illustrated in Fig. 6(a), the refractive index discloses a nonlinear behavior. It remains to unalter to 2.00 eV, and it progressively escalates and attains its first peak value of 1.47 at 7.59 eV for E||X and 1.44 at 7.69 eV for E⊥Z. After a specific oscillation, it makes a peak of 1.75 at 9.49 eV and 1.65 at 10.61 eV relating the orientation E||X and E⊥Z, respectively. The refractive index has a minimum value of 0.616 at 14.12 eV for parallel direction and 0.614 at 14.03 eV for perpendicular direction. After a few oscillations, it seems to be stable in the UV zone. The extinction coefficient K(ω) is correlated with the oscillating amplitude's damping of the incident electromagnetic wave's electric field. The extinction coefficient K(ω) has been illustrated in Fig. 6(b). In the extinction coefficient K(ω) spectrum curve, the maxima obtained at photon energies 10.03 eV, and 12.86 eV for E||X and 11.41 eV and 13.20 eV for E⊥Z. It means that at this particular energy value, the photons absorbed very fast by the material.

Fig. 7 illustrated the reflectivity and transmittance of the single-layer $MgCl_2$. In Fig. 7(a), it is clearly observed that the monolayer $MgCl_2$ shows reflectivity lower reflectivity less than 5% for the whole photon energy of electromagnetic radiation below the photon energy of 8 eV. Therefore, single-layer $MgCl_2$ transmits more than 95% EM radiation up to 8 eV photon energy (see Fig. 7(b). For the monolayer, the static value of the reflectivity (R(0); the value at photon energy 0 eV) is 1%. It was also seen that the reflectivity of monolayer $MgCl_2$ is found to be 2% below 4 eV photon energy and at the same photon energy the monolayer $MgCl_2$ transmits almost 98% EM radiations. Thus, the monolayer $MgCl_2$ may be applied as anti-reflecting material. The single-layer $MgCl_2$ has shown maximum reflectivity around 15% (at a photon energy of 13.26 eV) and 19% (at photon energy 13.66 eV) for the E||X and E⊥Z, respectively. A maximum of reflectivity, the minimum transmittance has been observed. This monolayer material shows the minimum transmittance at photon energy 13.26 eV in the direction of the parallel to the field (E||X) and at photon energy 13.66 eV in the direction perpendicular to the plane of field (E⊥Z).

3. Conclusions

In the present study, the structural, electronic, and optical properties of the single-layered $MgCl_2$ have been examined through the first-principles calculations. The 2D monolayer $MgCl_2$ in the H-phase of the 2D hexagonal lattice has a stable structure which has been confirmed by phonon dispersion spectra and AIMD calculations. Particularly, the 2D monolayer $MgCl_2$ has been gone through an indirect to direct bandgap transition when reducing the dimensionality from bulk to single-layer phase. The monolayer $MgCl_2$ has exhibited a direct bandgap of 7.38 eV. The 2D monolayer $MgCl_2$ is an optically transparent material because its refractive index values are very near to the water refractive index and have shown very small optical absorption in the infrared to near-ultraviolet region. Whereas a high optical absorption is found in the ultraviolet region therefore it is very useful for the ultraviolet-light absorber. Due to the presence of different polarization light along the in-plane and out-of-plane directions, the optical properties displayed anisotropic behavior. Also, the reflectivity values of 2D monolayer $MgCl_2$ have a maximum of 18% in the UV region, which means that most of the light is absorbed by materials. Our investigations suggest that the 2D monolayer $MgCl_2$ will be very useful in the field of high-performance optoelectronic nanodevices and atomically thin coating materials for preventing surface oxidation and corrosion.

Credit author statement

H. R. Mahida: Conceptualization, Formal analysis, Validation, Visualization, Writing – review & editing. Abhishek Patel: Methodology, Formal analysis, Writing – review & editing. Deobrat Singh: Conceptualization, Data curation, Formal analysis, Validation, Visualization, Writing – review & editing. Yogesh Sonvane: Writing – review & editing. P. B. Thakor: Supervision, Writing – review & editing. Rajeev Ahuja: Supervision, Funding acquisition, Software, Project administration, Writing – review & editing.

Declaration of competing interest

The authors declare that they have no known competing financial interests or personal relationships that could have appeared to influence the work reported in this paper.

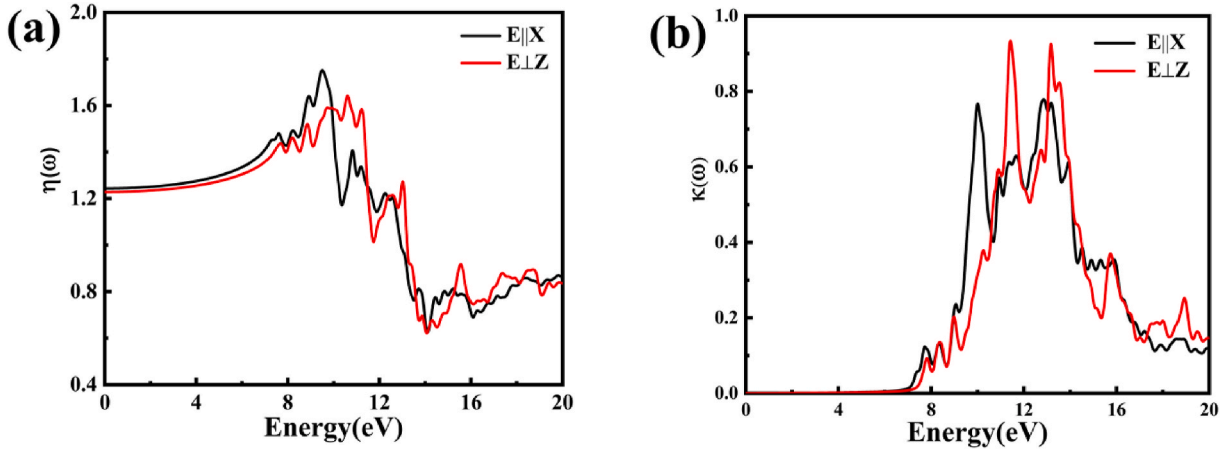

Fig. 6. (a) Refractive index and (b) extinction coefficient of the single layer $MgCl_2$.

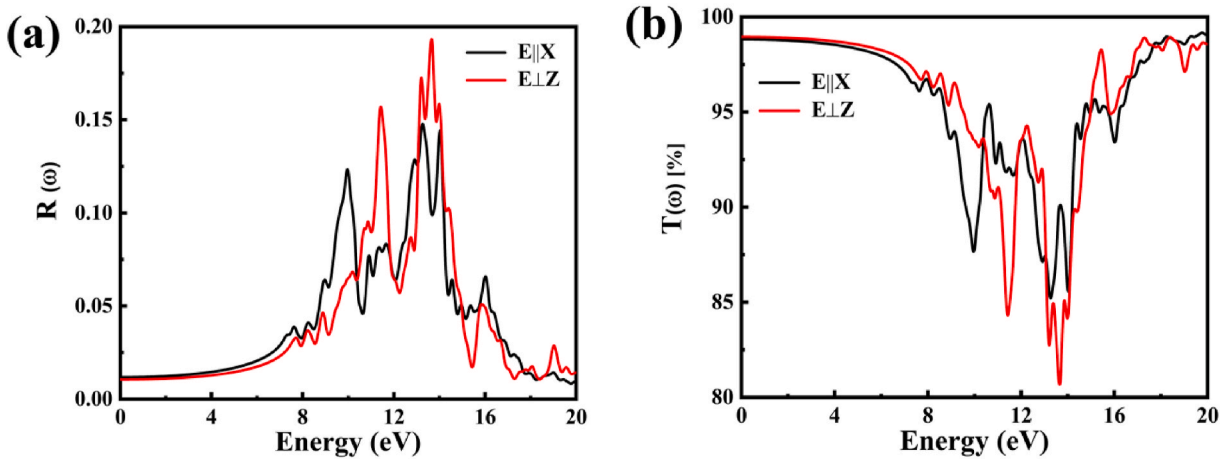

Fig. 7. (a) Reflectivity and (b) transmittance of the single-layer $MgCl_2$.

Acknowledgments

DS and RA thanks the Swedish Research Council (VR-2016-06014 & VR-2020-04410) and J. Gust. Richert stiftelse, Sweden (2021–00665) for financial support. AP is thankful to CSIR, India for his Junior Research Fellowship and financial support. YAS is thankful to the Science and Engineering Research Board (SERB), India, for the financial support (grant number: EEQ/2016/000217). SNIC and HPC2N are acknowledged for providing computing facilities.

References

[1] A.O.M. Almayyali, H.O. Muhsen, M. Merdan, M.M. Obeid, H.R. Jappor, Two-dimensional ZnI2 monolayer as a photocatalyst for water splitting and improvement its electronic and optical properties by strains, Phys. E Low-Dimensional Syst. Nanostructures. 126 (2021) 114487.
[2] A.O.M. Almayyali, B.B. Kadhim, H.R. Jappor, Stacking impact on the optical and electronic properties of two-dimensional MoSe2/PtS2 heterostructures formed by PtS2 and MoSe2 monolayers, Chem. Phys. 532 (2020) 110679.
[3] K. Khan, A.K. Tareen, M. Aslam, R. Wang, Y. Zhang, A. Mahmood, Z. Ouyang, H. Zhang, Z. Guo, Recent developments in emerging two-dimensional materials and their applications, J. Mater. Chem. C. 8 (2020) 387–440, https://doi.org/10.1039/C9TC04187G.
[4] E.P. Randviir, D.A.C. Brownson, C.E. Banks, A decade of graphene research: production, applications and outlook, Mater. Today 17 (2014) 426–432, https://doi.org/10.1016/j.mattod.2014.06.001.
[5] CHAPTER 1 the world of graphene, in: Nanoeng. Ski. Tools Mak. Technol. Invis., The Royal Society of Chemistry, 2020, pp. 1–60, https://doi.org/10.1039/9781839160363-00001.
[6] A. Ibrahim, A. Klopocinska, K. Horvat, Z. Abdel Hamid, Graphene-based nanocomposites: synthesis, mechanical properties, and characterizations, Polym 13 (2021), https://doi.org/10.3390/polym13172869.
[7] A. Bafekry, M. Faraji, M.M. Fadlallah, H.R. Jappor, N.N. Hieu, M. Ghergherehchi, S.A.H. Feghhi, D. Gogova, Prediction of two-dimensional bismuth-based chalcogenides Bi2X3 (X= S, Se, Te) monolayers with orthorhombic structure: a first-principles study, J. Phys. D Appl. Phys. 54 (2021) 395103.
[8] M.J. Abdulameer, S.S. Abed Al-Abbas, H.R. Jappor, Tuning optical and electronic properties of 2D ZnI2/CdS heterostructure by biaxial strains for optical nanodevices: a first-principles study, J. Appl. Phys. 129 (2021) 225104.

[9] A. Bafekry, M. Shahrokhi, A. Shafique, H.R. Jappor, F. Shojaei, S.A.H. Feghhi, M. Ghergherehchi, D. Gogova, Two-dimensional carbon nitride C6N nanosheet with egg-comb-like structure and electronic properties of a semimetal, Nanotechnology 32 (2021) 215702.

[10] M. Chhowalla, H.S. Shin, G. Eda, L.J. Li, K.P. Loh, H. Zhang, The chemistry of two-dimensional layered transition metal dichalcogenide nanosheets, Nat. Chem. 5 (2013) 263–275, https://doi.org/10.1038/nchem.1589.

[11] D. Geng, H.Y. Yang, Recent advances in growth of novel 2D materials: beyond graphene and transition metal dichalcogenides, Adv. Mater. 30 (2018) 1800865, https://doi.org/10.1002/adma.201800865.

[12] R. Li, Y. Cheng, W. Huang, Recent progress of janus 2D transition metal chalcogenides: from theory to experiments, Small 14 (2018) 1802091, https://doi.org/10.1002/smll.201802091.

[13] P. Mishra, D. Singh, Y. Sonvane, R. Ahuja, Two-dimensional boron monochalcogenide monolayer for thermoelectric material, Sustain. Energy Fuels 4 (2020) 2363–2369, https://doi.org/10.1039/d0se00004c.

[14] S. Kansara, S.K. Gupta, Y. Sonvane, Effect of strain engineering on 2D dichalcogenides transition metal: a DFT study, Comput. Mater. Sci. 141 (2018) 235–242, https://doi.org/10.1016/j.commatsci.2017.09.037.

[15] A. Patel, D. Singh, Y. Sonvane, P.B. Thakor, R. Ahuja, High thermoelectric performance in two-dimensional janus monolayer material WS-X (X = Se and Te), ACS Appl. Mater. Interfaces 12 (2020) 46212–46219, https://doi.org/10.1021/acsami.0c13960.

[16] A.S. Pawbake, J.O. Island, E. Flores, J.R. Ares, C. Sanchez, I.J. Ferrer, S.R. Jadkar, H.S.J. Van Der Zant, A. Castellanos-Gomez, D.J. Late, Temperature-dependent Raman spectroscopy of titanium trisulfide (TiS3) nanoribbons and nanosheets, ACS Appl. Mater. Interfaces 7 (2015) 24185–24190, https://doi.org/10.1021/acsami.5b07492.

[17] S. Hadji, A. Bouhemadou, K. Haddadi, D. Cherrad, R. Khenata, S. Bin-Omran, Y. Al-Douri, Elastic, electronic, optical and thermodynamic properties of Ba3Ca2Si2N6 semiconductor: first-principles predictions, Phys. B Condens. Matter 589 (2020) 412213.

[18] A. Mentefa, F.Z. Boufadi, M. Ameri, F. Gaid, L. Bellagoun, A.A. Odeh, Y. Al-Douri, First-principles calculations to investigate structural, electronic, elastic, magnetic, and thermodynamic properties of full-heusler Rh 2 MnZ (Z= Zr, Hf), J. Supercond. Nov. Magnetism 34 (2021) 269–283.

[19] S. LeBlanc, Thermoelectric generators: linking material properties and systems engineering for waste heat recovery applications, Sustain. Mater. Technol. 1 (2014) 26–35, https://doi.org/10.1016/j.susmat.2014.11.002.

[20] A. Patel, D. Singh, Y. Sonvane, P.B. Thakor, R. Ahuja, High thermoelectric performance in two-dimensional janus monolayer material WS-X (X = Se and Te), ACS Appl. Mater. Interfaces 12 (2020) 46212–46219, https://doi.org/10.1021/acsami.0c13960.

[21] A. Patel, D. Singh, Y. Sonvane, P.B. Thakor, R. Ahuja, Bulk and monolayer As2S3 as promising thermoelectric material with high conversion performance, Comput. Mater. Sci. 183 (2020) 109913, https://doi.org/10.1016/j.commatsci.2020.109913.

[22] H. Li, Y. Shi, M.H. Chiu, L.J. Li, Emerging energy applications of two-dimensional layered transition metal dichalcogenides, Nano Energy 18 (2015) 293–305, https://doi.org/10.1016/j.nanoen.2015.10.023.

[23] L. Ju, M. Bie, J. Shang, X. Tang, L. Kou, Janus transition metal dichalcogenides: a superior platform for photocatalytic water splitting, J. Phys. Mater. 3 (2020) 22004, https://doi.org/10.1088/2515-7639/ab7c57.

[24] A. Patel, D. Singh, Y. Sonvane, P.B. Thakor, R. Ahuja, Bulk and monolayer As_2S_3 as promising thermoelectric material with high conversion performance, Comput. Mater. Sci. 183 (2020), https://doi.org/10.1016/j.commatsci.2020.109913.

[25] Y. Li, C. Gao, R. Long, Y. Xiong, Photocatalyst design based on two-dimensional materials, Mater. Today Chem. 11 (2019) 197–216, https://doi.org/10.1016/j.mtchem.2018.11.002.

[26] J. Dong, X. Zhang, Chapter 2 - optical modulators based on 2D materials, in: Q. Bao, H.Y.B.T.-2D.M. for P, O.A. Hoh (Eds.), Woodhead Publ. Ser. Electron. Opt. Mater., Woodhead Publishing, 2020, pp. 37–77, https://doi.org/10.1016/B978-0-08-102637-3.00002-4.

[27] H.Y. Hoh, B.N. Shivananju, C.-M. Li, Q. Bao, Chapter 9 - 2D materials for bio-photonic applications, in: Q. Bao, H.Y.B.T.-2D.M. for P, O.A. Hoh (Eds.), Woodhead Publ. Ser. Electron. Opt. Mater., Woodhead Publishing, 2020, pp. 253–280, https://doi.org/10.1016/B978-0-08-102637-3.00009-7.

[28] B. Fadila, M. Ameri, D. Bensaid, M. Noureddine, I. Ameri, S. Mesbah, Y. Al-Douri, Structural, magnetic, electronic and mechanical properties of full-Heusler alloys Co2YAl (Y= Fe, Ti): first principles calculations with different exchange-correlation potentials, J. Magn. Magn Mater. 448 (2018) 208–220.

[29] K. Bidai, M. Ameri, I. Ameri, D. Bensaid, A. Slamani, A. Zaoui, Y. Al-Douri, Structural, mechanical and thermodynamic properties under pressure effect of rubidium telluride: first principle calculations, Arch. Metall. Mater. (2017).

[30] R. Chaurasiya, A. Dixit, R. Pandey, Strain-mediated stability and electronic properties of WS2, Janus WSSe and WSe2 monolayers, Superlattice. Microst. 122 (2018) 268–279, https://doi.org/10.1016/j.spmi.2018.07.039.

[31] D. Tyagi, H. Wang, W. Huang, L. Hu, Y. Tang, Z. Guo, Z. Ouyang, H. Zhang, Recent advances in two-dimensional-material-based sensing technology toward health and environmental monitoring applications, Nanoscale 12 (2020) 3535–3559, https://doi.org/10.1039/C9NR10178K.

[32] M. Idrees, H.U. Din, R. Ali, G. Rehman, T. Hussain, C. V Nguyen, I. Ahmad, B. Amin, Optoelectronic and solar cell applications of Janus monolayers and their van der Waals heterostructures, Phys. Chem. Chem. Phys. 21 (2019) 18612–18621, https://doi.org/10.1039/C9CP02648G.

[33] M. Donarelli, L. Ottaviano, 2D materials for gas sensing applications: a review on graphene oxide, MoS2, WS2 and phosphorene, Sensors 18 (2018), https://doi.org/10.3390/s18113638.

[34] B.-J. Wang, X.-H. Li, R. Zhao, X.-L. Cai, W.-Y. Yu, W.-B. Li, Z.-S. Liu, L.-W. Zhang, S.-H. Ke, Electronic structures and enhanced photocatalytic properties of blue phosphorene/BSe van der Waals heterostructures, J. Mater. Chem. A. 6 (2018) 8923–8929, https://doi.org/10.1039/C8TA01019F.

[35] A. Khireddine, A. Bouhemadou, S. Alnujaim, N. Guechi, S. Bin-Omran, Y. Al-Douri, R. Khenata, S. Maabed, A.K. Kushwaha, First-principles predictions of the structural, electronic, optical and elastic properties of the zintl-phases AE3GaAs3 (AE= Sr, Ba), Solid State Sci. 114 (2021) 106563.

[36] M. Ameri, F. Bennar, S. Amel, I. Ameri, Y. Al-Douri, D. Varshney, Structural, elastic, thermodynamic and electronic properties of LuX (X= N, Bi and Sb) compounds: first principles calculations, Phase Transitions 89 (2016) 1236–1252.

[37] X.-P. Zhai, B. Ma, Q. Wang, H.-L. Zhang, 2D materials towards ultrafast photonic applications, Phys. Chem. Chem. Phys. 22 (2020) 22140–22156, https://doi.org/10.1039/D0CP02841J.

[38] J. Yang, Y. Lu, Optical properties of phosphorene, Chin. Phys. B 26 (2017) 34201, https://doi.org/10.1088/1674-1056/26/3/034201.

[39] C. Si, Z. Sun, F. Liu, Strain engineering of graphene: a review, Nanoscale 8 (2016) 3207–3217, https://doi.org/10.1039/C5NR07755A.

[40] M.K. Zoubir, B. Fadila, B. Keltoum, A. Ibrahim, B.L. Farah, Y. Al-Douri, A. Mohammed, Structural, electronic and thermodynamic investigation of Ag2GdSi, Ag2GdSn and Ag2Gd Pb Heusler alloys: first-principles calculations, Mater. Test. 63 (2021) 537–542.

[41] M. Ameri, D. Hachemane, I. Ameri, B. Abidri, B. Bouhafs, D. Varshney, Y. Al-Douri, Structural, electronic, optical, and thermodynamic properties of copper halide CuCl1− xIx (0. 0≤ x≤ 1. 0) ternary alloy: first principal calculations, Chin. J. Phys. 53 (2015) 40802.

[42] K. Bidai, M. Ameri, A. Zaoui, I. Ameri, Y. Al-Douri, First principle study of mechanical stability and thermodynamic properties of anti-fluorite Li2O and Rb2O under pressure and temperature effect, Chin. J. Phys. 54 (2016) 678–694.

[43] Y. Li, M. Dailey, P.J. Lohr, A.D. Printz, Performance and stability improvements in metal halide perovskite with intralayer incorporation of organic additives, J. Mater. Chem. A. 9 (2021) 16281–16338, https://doi.org/10.1039/D1TA05252G.

[44] Z. Jin, Z. Zhang, J. Xiu, H. Song, T. Gatti, Z. He, A critical review on bismuth and antimony halide based perovskites and their derivatives for photovoltaic applications: recent advances and challenges, J. Mater. Chem. A. 8 (2020) 16166–16188, https://doi.org/10.1039/D0TA05433J.

[45] N. Guechi, A. Bouhemadou, Y. Medkour, Y. Al-Douri, R. Khenata, S. Bin-Omran, Electronic and thermoelectric properties of the layered Zintl phase CaIn2P2: first-principles calculations, Philos. Mag. A 100 (2020) 3023–3039.

[46] A. Moussali, M.B. Amina, B. Fassi, I. Ameri, M. Ameri, Y. Al-Douri, First-principles calculations to investigate structural and thermodynamic properties of Ni 2 Laz (Z= As, Sb and Bi) Heusler alloys, Indian J. Phys. 94 (2020) 1733–1747.

[47] P. Löbmann, Sol-gel processing of MgF2 antireflective coatings, Nanomaterials 8 (2018), https://doi.org/10.3390/nano8050295.

[48] D. Bernsmeier, J. Polte, E. Ortel, T. Krahl, E. Kemnitz, R. Kraehnert, Antireflective coatings with adjustable refractive index and porosity synthesized by micelle-templated deposition of MgF2 sol particles, ACS Appl. Mater. Interfaces 6 (2014) 19559–19565, https://doi.org/10.1021/am5052685.

[49] H.R. Mahida, D. Singh, Y. Sonvane, S.K. Gupta, P.B. Thakor, MgF2 monolayer as an anti-reflecting material, Solid State Commun. 252 (2017) 22–28, https://doi.org/10.1016/j.ssc.2017.01.005.
[50] G. Kresse, J. Furthmüller, Efficiency of ab-initio total energy calculations for metals and semiconductors using a plane-wave basis set, Comput. Mater. Sci. 6 (1996) 15–50, https://doi.org/10.1016/0927-0256(96)00008-0.
[51] G. Kresse, J. Furthmüller, Efficient iterative schemes for ab initio total-energy calculations using a plane-wave basis set, Phys. Rev. B Condens. Matter 54 (1996) 11169–11186, https://doi.org/10.1103/PhysRevB.54.11169.
[52] D. Joubert, From ultrasoft pseudopotentials to the projector augmented-wave method, Phys. Rev. B Condens. Matter 59 (1999) 1758–1775, https://doi.org/10.1103/PhysRevB.59.1758.
[53] J.P. Perdew, K. Burke, M. Ernzerhof, Generalized gradient approximation made simple, Phys. Rev. Lett. 77 (1996) 3865–3868, https://doi.org/10.1103/PhysRevLett.77.3865.
[54] H.J. Monkhorst, J.D. Pack, Special points for Brillouin-zone integrations, Phys. Rev. B 13 (1976) 5188–5192, https://doi.org/10.1103/PhysRevB.13.5188.
[55] T.M. Henderson, J. Paier, G.E. Scuseria, Accurate treatment of solids with the HSE screened hybrid, Phys. Status Solidi 248 (2011) 767–774.
[56] J. Heyd, G.E. Scuseria, M. Ernzerhof, Hybrid functionals based on a screened Coulomb potential, J. Chem. Phys. 118 (2003) 8207–8215, https://doi.org/10.1063/1.1564060.
[57] J. Heyd, J.E. Peralta, G.E. Scuseria, R.L. Martin, Energy band gaps and lattice parameters evaluated with the Heyd-Scuseria-Ernzerhof screened hybrid functional, J. Chem. Phys. 123 (2005) 174101, https://doi.org/10.1063/1.2085170.
[58] H. Shang, C. Carbogno, P. Rinke, M. Scheffler, Lattice dynamics calculations based on density-functional perturbation theory in real space, Comput. Phys. Commun. 215 (2017) 26–46, https://doi.org/10.1016/j.cpc.2017.02.001.
[59] A. Togo, I. Tanaka, First principles phonon calculations in materials science, Scripta Mater. 108 (2015) 1–5, https://doi.org/10.1016/j.scriptamat.2015.07.021.
[60] D. Singh, S.K. Gupta, Y. Sonvane, I. Lukačević, Antimonene: a monolayer material for ultraviolet optical nanodevices, J. Mater. Chem. C. 4 (2016) 6386–6390, https://doi.org/10.1039/C6TC01913G.
[61] H.R. Mahida, D. Singh, Y. Sonvane, P. Thakor, R. Ahuja, S. Gupta, The influence of edge structure on the optoelectronic properties of Si2BN quantum dot, J. Appl. Phys. 126 (2019), https://doi.org/10.1063/1.5131149, 0.
[62] D. Singh, V. Shukla, R. Ahuja, Optical excitations and thermoelectric properties of two-dimensional holey graphene, Phys. Rev. B 102 (2020) 75444, https://doi.org/10.1103/PhysRevB.102.075444.